Rather et al

Research Article format

Key words: Mitochondria, nucleus, programmed cell death, phagocytosis

Summary Statement (29 words): This work describes the genetic control and cellular dynamics of a factor linked to cancer, metabolic and degenerative disease acting in developmentally dying cells to instruct their own removal.

Running title (31 characters): WAH-1/AIF phagocytic dynamics

Working title (108 characters):

EOR-1/PLZF-regulated WAH-1/AIF sequentially promotes early and late stages of non-apoptotic corpse removal

Nathan Rather[1], Melvin Williams[2], Aladin Elkhalil[1], Karen Juanez[1], Rashna Sharmin[1], Ginger Clark[1], Shai Shaham[2], Piya Ghose[1*]

[1]The University of Texas at Arlington

[2]The Rockefeller University

*To whom correspondence should be addressed.

piya.ghose@uta.edu

Abstract (180 words)

Programmed cell death (PCD) is a crucial, genetically-encoded, and evolutionarily-conserved process required for development and homeostasis. We previously identified a genetically non-apoptotic, highly ordered, and stereotyped killing program called Compartmentalized Cell Elimination (CCE) in the *C. elegans* tail-spike epithelial cell (TSC). Here we identify the transcription factor EOR-1/PLZF as an important coordinator of CCE. Loss of EOR-1 results in a large, persisting, un-engulfed soma with enlarged nuclei. We find that EOR-1 and its partners positively regulate the transcription of the Apoptosis Inducing Factor AIF homolog, WAH-1/AIF. We report stereotyped and sequential spatiotemporal

dynamics of WAH-1/AIF1 during phagocytosis, with defined roles acting early and late, within the dying cells. Mitochondria to plasma membrane translocation within the TSC soma is required its internalization by its phagocyte, and plasma membrane to nuclear translocation is required for DNA degradation and ultimately, corpse resolution. Our study suggests that EOR-1 serves as a master regulator for the transcriptional control of DNA degradation is essential for changes in nuclear morphology required for cellular dismantling and infers that tight spatiotemporal regulation of WAH-1/AIF is required for this function.

Introduction

Programmed cell death (PCD) is a genetically-encoded and evolutionarily-conserved cell elimination vital for normal development and homeostasis (1), with defects linked to disease (2-4). Apoptosis, the most well-studied form of PCD, is by defined by cell shrinkage, chromatin condensation, nuclear fragmentation, and mitochondrial fragmentation (1, 5, 6). Genetically, apoptosis is controlled by several conserved regulators, including the cysteine protease caspase family. Caspases have a conserved pathway of regulators, including the pro-apoptotic Apaf-1, the antiapoptotic Bcl-2, and the proapoptotic BH3-only in mammals (7-9). Several forms of non-apoptotic cell death have been also described (10).

In addition to the cell killing, cell remains must be efficiently removed via phagocytosis to avoid secondary necrosis and autoimmune consequences (11, 12). The mechanism of apoptotic corpse phagocytosis is well described. First, the dying cells are recognized (13), and engulfed (14); once fully internalized and encapsulated in a phagocytic vesicle called a phagosome, the corpse is eventually resolved through multiple steps of increased acidification of the phagosome (15) and introduction of lysosomal hydrolases (16). Apoptotic engulfment and phagosome maturation pathways are conserved in mammals (17, 18).

Much of what we know about apoptotic cell killing and clearance has been gleaned using the powerful genetic model organism, the nematode *C. elegans* (19) (20). Phagocytosis has also been extensively characterized in the nematode, with seminal work conducted on the molecular machinery and cell biology required for corpse engulfment (21) and phagosome maturation (22). Newer studies have described the role of engulfment machinery genes in neuronal sculpting and function (23), in polar body removal (24), and in cell clearance following LCD and other deaths (25, 26).

We previously described the molecular pathway required for the Compartmentalized Cell Elimination (CCE) of the tail-spike epithelial scaffolding cell (TSC) in the *C. elegans* embryo, a tripartite cell killing program required for the death and clearance of complex cells (27). Briefly, CCE entails three distinct and stereotyped cell elimination events. As the CCE program occurs 10 times slower than most apoptotic nematode cells, it allows for detailed examination of these events at the gross and subcellular

level (27). During CCE, the single process of the TSC segments into two morphologically distinct sub-compartments that exhibit degenerative morphologies resembling two different forms of neurite pruning (27). The binucleate soma rounds, superficially resembling apoptotic morphology (27). The highly specialized morphology of the TSC allows it to serve as a timekeeper for the steps of CCE.

Molecularly, CCE is genetically distinct from apoptosis (28-30). While it does require the *C. elegans* caspase CED-3, it is not regulated by the BH3-only homolog EGL-1 (30), and additional non-canonical regulators are required for cell killing (28-30) During engulfment, the canonical engulfment machinery operates only on the soma corpse (27). Dismantling of the TSC process remnants instead require the cell-cell fusogen EFF-1 for phagosome sealing (27).

In the present study, we identify EOR-1/PLZF as the first transcriptional regulator of a cell clearance regulator, the homolog of the Apoptosis inducing factor WAH-1. We characterize WAH-1 dynamics and subcellular localization and define dual roles in sequential steps of cell corpse removal. We find that EOR-1-regulated WAH-1 acts in the dying TSC to promote the careful timing of both corpse internalization and resolution. Failure of EOR-1/PLZF and/or WAH-1/AIF function leads to a corpse progression transition state, characterized by lack of cellular engulfment and failure of lysosomal corpse degradation.

Results

The transcription factor EOR-1/PLZF promotes CCE compartment-specifically

The TSC **(Figure 1A**) extends a single posteriorly-directed process when intact (IMA, intact, mature). During early CCE (BA, beading, attached; BD, beading, detached), this single process shows axon pruning-like morphology proximally and axon retraction-like pruning distally (**Figure 1B**). At this step, the binucleate soma rounds in a manner superficially resembling apoptotic cell death. Later in CCE, the distal process retracts into a distal node (**Figure 1C**) (soma, distal retraction, SDR) leaving behind a soma and a distal remnant (soma, distal degrading, SDD) (**Figure 1D**) which are phagocytosed stochastically by different neighboring phagocytes before the animal hatches. The highly organized and stereotyped elimination sequence of CCE allows us to use the cell's general morphology as a timekeeper for events in the cell death program.

While CCE is dependent on the main *C. elegans* caspase CED-3 (27) it is genetically distinct from apoptosis as it does not require EGL-1/BH3-only (30) CCE is also temporally distinct from apoptosis as it takes longer to complete. While most cells fated to die apoptotically in *C. elegans* live for only 30 minutes (31), the TSC lives for 5 hours (32) with CCE of the TSC taking 150 minutes (27). This longer timescale positions CCE of the TSC as a promising platform to better understand the fundamental cell biology of programmed cell elimination in greater detail.

We performed a forward genetic screen for CCE defects of the TSC using a membrane marker strain for the TSC (TSC-myrGFP) that we have previously employed (27). We obtained a mutant, *ns957,* bearing an inappropriately persisting and enlarged cell body only, but with no process **(Figure 1E)**. This CCE defect increased when animals were raised and scored at 25ºC when compared to 20ºC **(Figure 1F)**.

Intrigued by a mutant where only soma elimination fails but where the process is successfully eliminated, we examined the morphology of our mutant more carefully using Differential Interference Contrast (DIC) microscopy. Apoptotic cell death has well-documented morphological characteristics that are visible under DIC microscopy, such as pyknotic nuclei and refractility (33). However, we observed in our *ns957* mutant enlarged and non-pyknotic nuclei, and a non-refractile cytoplasm (**Figure 1G-G"**).

Following Whole Genome Sequencing, genomic DNA rescue (**Figure 1I**), and examination of other alleles (**Figure 1J, K-K'**), we found that our screen mutant has a causative lesion in the gene encoding the transcription factor EOR-1/PLZF, resulting in an E570K change in the Zn finger domain (**Figure 1H**). We also found from cell-specific rescue experiments that *eor-1* acts cell-autonomously in the TSC (**Figure 1L**) and that *eor-1* is expressed in the nucleus, consistent with the notion that it acts as a transcription factor (**Figure 1M**).

EOR-1 is the ortholog of the BTB/zinc-finger tumor-suppressor transcription factor PLZF and has been reported to be a regulator for both apoptotic and non-apoptotic (LCD) forms of PCD identified in *C. elegans* (34). In a non-cell death context, EOR-1 is involved in neuronal specification (35). However, in terms of PCD, EOR-1/PLZF has been implicated both in the apoptotic deaths of the HSN neurons (34) as well as in non-apoptotic Linker-type Cell Death (LCD) (36). EOR-1 appears to play a specification role upstream to the execution phase of these deaths, acting upstream or in parallel to CED-9 in the HSNs and upstream of HSF-1 in conjunction with WNT signaling in LCD (34). However, its precise mechanistic contribution to either form of PCD remains unknown.

EOR-1/PLZF acts downstream of CED-3/Caspase, but with known regulatory partners

We proceeded to examine the precise role of EOR-1 in PCD using CCE of the TSC as our model. In its known roles in cell fate, EOR-1 functions with known co-regulators of transcription. We first examined a role of EOR-2, which binds to the BTB domain of EOR-1 and promotes its function, (37) by looking at *eor-2 (cs42)* mutants (**Figure 2A, B, C**) and found that this phenocopied *eor-1* mutants. EOR-1/PLZF has also been reported to act as a pioneer transcription factor that functions in conjunction with the MAU-2 cohesin loader, and the SWSN-1 SWI/SWNF chromatin remodeling complex member to modify chromatin architecture and gene expression of genes required for the maturation of the post-mitotic development of HSN neurons (35). To determine whether EOR-1 functions with MAU-2 and SWSN-1 to promote CCE, we examined *mau-2 (qm160)* **(Figure 2A, D, E*)*** and *swsn-1 (ku355)* **(Figure**

2A, F, G) mutant larvae; we found that they show persisting TSC somas that phenocopy the distinct morphology of *eor-1* mutant animals. Therefore, EOR-1 functions in the new setting of CCE via its previously identified partners in transcription.

We next asked whether EOR-1 functions upstream or downstream of CED-3/caspase and whether it impacts TSC fate in a more general way. As in the case of apoptosis, CCE requires the main *C. elegans* caspase CED-3, as well as its upstream regulator CED-4/Apaf1(30). We generated a *ced-4(n1162); eor-1(cs28)* double mutant and found an intact TSC phenotype and nuclear phenotype characteristic of *ced-3(n717)* single mutants (N=10/10), suggesting that EOR-1 acts downstream of CED-4 and CED-3 to promote CCE and likely does not affect TSC development **(Figure 2H-H', I-I').**

EOR-1/PLZF is important late in CCE for corpse internalization

Given the striking soma morphology of *eor-1* mutants, we examined closely the soma morphology changes across the different CCE stages in both wild-type and *eor-1 (cs28)* mutants using a combination of DIC optics and our fluorescent TSC membrane reporter, and noted TSC soma features at different CCE stages. Prior to CCE, when the cell has matured, but is still intact (Intact mature stage, IMA) (**Figure 3A-B"**), the soma appears polygonal with its nuclei appearing ovoid, flat and speckled with many small refractile bodies (**Figure 3B'-B"**). As CCE sets in, the soma becomes round and the proximal process displays beading (Beading attached stage, BA) (**Figure 3C-D"**), during which the nuclei appear round and spheroid (**Figure 3D'-D"**). Nuclear contents retain a speckled appearance of refractile material.

As CCE progresses to the next stage (soma-distal process retracting stage, SDR) (**Figure 3E-F'**), the junction between the rounded soma detaches from the beading proximal process (**Figure 3E**) and the distal process starts to retract into a node. At this stage, nuclei are rounded with intranuclear contents beginning to condense into more discrete areas (**Figure 3F'-F"**). The soma and distal process are then removed by separate phagocytes. At this stage, the soma forms a classic refractile, button-like appearance as it starts to be engulfed. After the SDR/retraction stage, the soma and process appear superficially to be degrading (Soma-distal process degrading stage, SDD) (**Figure 3G-H"**). The soma at this point appears non-refractile and vacuolized, with its nuclei appearing pyknotic and detached **(Figure 3H'-H"**). Apoptosis and other forms of PCD are defined by subcellular hallmarks such as specific changes in nuclear morphology and cell enlargement. We find that, during CCE, pyknotic nuclei appear also to exhibit Brownian motion within the non-refractile cytoplasm **(Figure 3H'-H"**). The TSC membrane appears diffuse at this stage and the membrane loses its discrete ring surrounding the cell. We examined *eor-1(cs28)* TSCs in a similar manner and found that CCE progression appeared normal up until the SDD/soma-distal process degrading stage, where the nuclei fail to condense and the membrane does not lose its integrity (**Figure 3I-P"**).

174 We next compared the *eor-1(ok1127)* mutant defect with that of mutants for caspase/cell killing,
175 *ced-3(n717)* and engulfment, *ced-12(ky149),* and performed epistasis experiments. We compared the
176 soma-persistence defects of *ced-3(n717)* (**Figure 4 A-A"**), *ced-12(ky149)* (**Figure 4 B-B"**) and *eor-1*
177 mutants (**Figure 4C-C"**). We observed that the TSC soma morphological features of *eor-1* were distinct
178 from both *ced-3 (n717)* and *ced-12(ky149)* mutants, suggesting the cell is neither living nor engulfed.
179 Moreover, a double mutant for *eor-1* and *ced-12(ky149)* (**Figure 4D-D"**) phenocopied the *eor-1 (ok1127)*
180 single mutants, rather than the refractile corpse of *ced-12(ky149)* mutants. This supports the idea that
181 the persisting soma of *eor-1* mutants has progressed through the killing steps of CCE but has not been
182 engulfed and is consistent with an arrest at the SDD stage. We examined whether the persisting corpse
183 of *eor-1 (cs28)* mutants is internalized by its neighboring phagocyte. We used a cytosolic reporter
184 labelling the TSC soma's neighboring phagocyte (*skn-1p*::mKate2) and found that the persisting soma
185 *eor-1* **(Figure 4E-G; Supplemental Movie S1**) mutants remains outside the phagocyt*e (*N=10/12*),*
186 suggesting failure of corpse internalization.
187
188 **EOR-1/PLZF positively regulates *wah-1*/Aif expression in the TSC**
189 We next sought to identify the transcriptional target for EOR-1/PLZF in the context of CCE and
190 examined published data obtained from a previous ChiP-Seq analysis study of EOR-1/PLZF
191 transcriptional targets (38). We noted the gene *wah-1,* which encodes a homolog of the mitochondrial
192 flavoprotein Apoptosis Inducing Factor AIF1, a multifunctional enzyme that is essential for mitochondrial
193 bioenergetic function (39). Interestingly, WAH-1 has been shown to function to promote apoptotic cell
194 death in the *C. elegans* germline (40, 41). Upon activation by CED-3/Caspase and EGL-1/BH3-only,
195 WAH-1/AIF promotes apoptosis through DNA degradation via CPS-6 endonuclease activation (41).
196 WAH-1/AIF has also been shown to aid in phosphatidylserine (PS) exposure by promoting SCRM-1
197 scramblase function (40) to facilitate apoptotic corpse recognition.
198 We tested the hypothesis that EOR-1/PLZF promotes CCE through the transcriptional activation
199 of *wah-1*. First, we assessed whether *wah-1* was required to promote CCE. We found that *wah-1*
200 (*gk5392*) mutants phenocopy *eor-1* mutants (**Figure 5A, B**), and the double mutant is not additive (**Figure**
201 **5B, N=150**). We also found from cell-specific rescue experiments that *wah-1* functions in the TSC (**Figure**
202 **5C, N=150)**. We examined an endogenous reporter for *wah-1* (*wah-1*p::WAH-1::GFP) at the intact
203 mature (IMA) embryo stage in wild-type (**Figure 5D)**, *eor- 1(cs28)* (**Figure 5E**), *mau- 2 (qm160)* (**Figure**
204 **5F)**, and *swsn-1(os22)* (**Figure 5G**) mutants and found decreased levels of *wah-1* expression in mutants
205 (**Figure 5H**). These data support the notion that WAH-1 promotes CCE by acting within the TSC and that
206 it is transcriptionally regulated by EOR-1, MAU-2 and SWqSN-1. This is supported by modENCODE data
207 for *wah-1,* which identified an EOR-1 binding sequence at the *wah-1* promoter site(42). Additionally, as
208 *wah-1* contains an HTZ-1 histone binding site, and as cohesin loaders require nucleosome-free loci to

209 bind, our finding further implicates the importance of EOR-1 and its associated chromatin remodeling
210 complex proteins in maintaining *wah-1* transcription during death.
211
212 **WAH-1 functions in corpse internalization**
213 We first considered WAH-1's possible role at the plasma membrane, as the soma rounds. Prior
214 studies have shown that WAH-1/AIF promotes apoptotic corpse recognition and engulfment (40). We
215 looked at CCE progression in *wah-1*(*gk5392*) (**Figure 6A-H"**) mutants and found that the progression
216 differed from wild-type, arresting, as in *eor-1* mutants, at the SDD stage (**Figure 6G-H"**).
217 Next, we used a cytosolic reporter labelling the neighboring phagocyte (*skn-1*p::mKate2) and
218 found that the persisting soma of *wah-1* mutants remains outside the phagocyte **(Figure 6I-K**, N=11/13),
219 similar to *eor-1* mutants and that both *eor-1* and *wah-1* mutants the phagocyte pseudopods are not
220 formed (**Figure 4E-G, Supplemental Movie S1; Figure 6I-K; Supplemental Movie S2**), suggesting
221 failure in corpse recognition.
222 WAH-1 has been shown to promote SCRM-1 scramblase flipping of phosphatidylserine from the
223 inner to the outer plasma membrane (40). We found that *scrm-1(-)* mutants also displayed CCE defects
224 (**Figure 6 L, M, N=9)** akin to *eor-1* and *wah-1* mutants. These data suggest WAH-1 is important for TSC
225 soma corpse recognition during CCE in a manner dependent on SCRM-1, as seen in its apoptotic role.
226
227 **WAH-1 also functions in nuclear dismantling after corpse internalization**
228 WAH-1 has been shown to be involved in DNA degradation and to translocate from the
229 mitochondria to the nucleus (41). We tested whether this is true during CCE and attempted to separate
230 WAH-1 function in corpse internalization versus its possible nuclear role.
231 WAH-1 has been shown to promote DNA degradation during apoptosis by acting to enhance the
232 activity of the CPS-6/Endonuclease G nuclease (41, 43). We found that *cps-6* mutants also phenocopy
233 *wah-1* and *eor-1* mutants for CCE (**Figure 7A, B, N=6).** Moreover, a *wah-1; cps-6* double mutant did not
234 show an increase in TSC defects (**Figure 7A**) suggesting these genes function in the same genetic
235 pathway. We also found that mutants for *nuc-1*, a lysosomal acid hydrolase that promotes late DNA
236 degradation (44, 45), also phenocopy *eor-1* and *wah-1* mutants (**Figure 7A, C)** supporting a role for
237 WAH-1 in DNA degradation. Interestingly, it has been reported that degradation of apoptotic cell corpse
238 DNA requires contributions of both the dying and the engulfing cell. NUC-1 is released from the apoptotic
239 corpse into the phagolysosome, assisting in DNA degradation within the engulfing cell (45).
240 As such, we investigated whether *cps-6* mutants arrested in the phagosome maturation stage.
241 Interestingly, unlike in *wah-1* and *eor-1* mutants, the soma of *cps-6* mutants appears to be internalized
242 (**Figure 7D-F; Supplemental Movie S3**) (N=9/10), suggesting that CPS-6/EndoG is not involved in

243 WAH-1's corpse internalization function and, rather, likely plays a role in nuclear degradation downstream
244 of internalization during phagosome maturation to resolve the internalized corpse.
245 To test in which stage of phagosome maturation WAH-1 and CPS-6 function together, we looked
246 at known markers of phagosome maturation, for early (GFP::RAB-5) (**Figure 7G-G"**), late (GFP::RAB-7)
247 (**Figure 7H-H"**) and phagolysosomes (LAAT-1::mCherry) (**Figure 7I-I"**)(27) in *cps-6* mutants.We found
248 that the phagosome bearing the internalized corpse is decorated by LAAT-1, suggesting arrest at the
249 phagolysosomal stage; in contrast, localization of RAB-5 and RAB-7 were normal. This is consistent with
250 a role of NUC-1 in TSC DNA degradation and supports previous hypotheses about NUC-1 being a
251 phagolysosomal substrate. This also suggests that a defect in corpse degradation causes the dramatic
252 nuclear and cytoplasmic phenotypes in mutants.
253
254 **Defined spatiotemporal dynamics suggest dual functions of WAH-1/AIF before and after corpse**
255 **internalization**
256 Having identified WAH-1/AIF as a regulator of CCE at both the level of corpse internalization and
257 degradation, we examined its localization pattern across CCE stages (**Figure 8)**. First, we examined TSC
258 mitochondrial localization against the TSC plasma membrane. Interestingly, we found mitochondria to be
259 close to the plasma membrane through most of CCE (**Figure 8 A-D**), appearing fragmented at the SDD
260 stage when the plasma membrane integrity is lost (**Figure 8D**). We then examined TSC promoter-driven
261 WAH-1::mCherry against a TSC promoter-driven mitochondrial matrix marker (**Figure 8E-H"**). When the
262 cell is intact, WAH-1 appears to be mitochondrial (**Figure 8E-E"**) and not in the plasma membrane.
263 However, as the beading (BA/BD) stage begins, the soma rounds and the soma detaches from the
264 process, both mitochondria and WAH-1 appear to be at or close to the plasma membrane (**Figure 8 F-**
265 **G"**). Afterwards, at the SDD stage, WAH-1 is not seen at the plasma membrane but can be seen in what
266 appears to be fragmented mitochondria (**Figure 8H-H"**); however, it is largely delocalized and
267 cytoplasmic.
268 We imaged our TSC reporter against the soma-phagocyte reporter in wild-type embryos (**Figure**
269 **8I-X)** to examine whether the TSC soma is outside the phagocyte at the IMA stage (**Figure 8I-L)** We
270 found that the TSC soma is internalized from what we define as the BD (beading, detached) stage when
271 the soma rounds and appears refractile (**Figure 8M-P**) through the SDR (**Figure 8Q-T**) and SDD (**Figure**
272 **8U-X**) stages. We observe WAH-1 outside of mitochondria at the SDD stage (**Figure 8D** and **8U-X**) after
273 being at the mitochondria and plasma membrane earlier at the SDR (**Figure 8C** and **8Q-T**) and BD
274 (**Figure 8B** and **8M-P**) stages. Together, these data suggest that a physical association between
275 mitochondria and the plasma membrane, possibly involving WAH-1, may be important early in
276 phagocytosis and that exit of WAH-1 from mitochondria may be important for corpse degradation and
277 digestion after internalization.

Discussion

Here we describe defined subcellular events of cell corpse during phagocytosis. Our work supports a model (**Figure 9)** in which WAH-1/AIF dual functions, positively regulated by EOR-1/PLZF, ensure clearance of the TSC soma corpse during CCE. We provide the first evidence of transcriptional regulation of WAH-1. It will be interesting to explore whether the same transcriptional relationship between EOR-1 and *wah-1* exists in other forms of PCD such as LCD. We describe previously unreported morphological features of programmed cell elimination. Our study expands on prior studies linking EOR-1/PLZF to apoptotic (34) and non-apoptotic (36) PCD by providing a precise mechanistic contribution of EOR-1/PLZF in CCE and implies that programmed cell degradation occurs in a highly regulated manner, not by just via catastrophic destruction. We also propose that regulation of DNA degradation and nuclear destruction allows the corpse to act as an active player in its own destruction, coordinating with the engulfing cell.

Notably, WAH-1 exit from mitochondria is reported to be dependent on EGL-1/BH3-only (41). However, CCE is independent of EGL-1/BH3-only (30). The WAH-1 localization pattern suggests WAH-1 can promote nuclear degradation independent of EGL-1. The lack of EGL-1 involvement may affect WAH-1's ability to be released from mitochondria and may explain why WAH-1 is still associated to some degree with mitochondria until the SDD stage of CCE. The lack of EGL-1 may cause WAH-1's mitochondrial release to be markedly slower, which may explain why the time course of CCE is much longer than apoptotic germline cells.

Our work also opens several exciting questions . What guides WAH-1 translocation to the plasma membrane and nucleus in a temporally regulated manner? Does phosphatidylserine triggers engulfment during CCE? What is the molecular mechanism by which WAH-1/AIF transduces the signal from the changing phagosomal environment to respond via nuclear translocation to execute its role in DNA and nuclear degradation? How does WAH-1/AIF know to translocate so specifically in the corpse at distinct phagosomal stages? We also suggest that failure to appropriately degrade DNA can lead severe exaggerations in nuclear morphology. Taken together, our study expands our understanding of the transcriptional regulation of corpse clearance and highlights roles for regulators of apoptosis in in broader contexts of programmed cell elimination.

Materials and Methods

C. elegans methods

C. elegans strains were cultured using standard methods on *E. coli* OP50 and grown at 20ºC. Wild-type animals were the Bristol N2 subspecies. For most TSC experiments, one of two integrated reporters were

313 used: *nsIs435=TSCp::myrGFP* or *nsIs685=TSCp::mKate2-PH.* In addition, *nsIs650=wah-1*p::WAH-
314 1::GFP was used. Integration of extrachromosomal arrays was performed using UV and trioxsalen
315 (T2137, Sigma). Animals were scored at 20ºC, unless otherwise mentioned.
316
317 **Imaging**
318 Images were collected on a Nikon TI2-E Inverted microscope using a CFI60 Plan Apochromat Lambda
319 60x Oil Immersion Objective Lens, N.A. 1.4 (Nikon) and a Yokogawa W1 Dual Cam Spinning Disk
320 Confocal images were acquired using NIS-Elements Advanced Research Package. For still embryo
321 imaging, embryos were anesthetized using 0.5 M sodium azide. Larvae were paralyzed with 10mM
322 sodium azide. Widefield imaging was performed on a Carl Zeiss Axio Imager.M2 microscope with 63X oil
323 immersion lens. Super-resolution images were taken using a VTiSIM Super resolution Live Cell Confocal
324 Imaging System.
325
326 **Quantifying CCE defects**
327 TSC death defects were scored at the L1 stage. Animals were mounted on slides on 2% agarose-M9
328 pads, paralyzed with 10mM sodium azide, and examined on a Carl Zeiss Axio Imager.M2 microscope
329 with 63X oil immersion lens. The persisting TSC was identified by fluorescence based on its location and
330 morphology. At least 50 animals were scored per genotype. For images, each image is representative of
331 10 sampled.
332
333 **Worm strains used in this study**
334 List gene alleles under different chromosomes linkage groups (LG I-X)
335 LGI: *ced-12(ky149), mau-2(qm160), scrm-1(tm698), cps-6(ok1718)*
336 LGII:
337 LGIII*: ced-4(n1162), wah-1 (gk5392)*
338 LGIV: *eor-1(ok1127), eor-1(cs28), ced-3(n717)*
339 LGV: *swsn-1(os22)*
340 LGX: *eor-2 (cs42) nuc-1 (e1392)*
341
342 **Plasmids and Transgenics**

343 Plasmids were generated via Gibson cloning. Primer sequences and information on the construction of
344 plasmids used in this study are provided in (**Supplemental Table 1**). The full list of transgenes is
345 described in (**Supplemental Table 2**). The full length or fragment of the *aff-1* promoter was used to label
346 the TSC.

347 **Quantification of WAH-1::GFP fluorescence intensity**

348 Images of the intact TSC in animals harboring *wah-1* promoter driven *wah-1*::GFP in WT, *eor-1(cs28)*,
349 *mau-2(qm160)*, and *swsn-1(os22)* were collected using confocal microscopy as stated above using the
350 same settings across all images. Sum intensity projections of the TSC soma were generated by following
351 TSCp::mCherry in Fiji Image J software and GFP intensity was then calculated using this software. CTCF
352 was calculated using Microsoft Excel and graphed using Graphpad. All data points represent the average
353 of 10 animals. Statistical significance was determined by Mann-Whitney U test for comparison between
354 wild type and mutant animals.

355

356 **Statistics**

357 Sample sizes and statistics were based on previous studies of CCE and the TSC(27). Independent
358 transgenic lines were treated as independent experiments. An unpaired two-tailed *t*-test was used for all
359 persisting TSC quantifications (GraphPad Prism). For all figures, mean ± standard error of the mean
360 (s.e.m.) is represented. P-values are indicated in (**Supplemental Table 3**)

361

362 **Acknowledgments:**

363 We thank Dr. Jennifer Malin for comments on the manuscript. NR and PG designed the experiments and
364 wrote the manuscript. NR, MW, KJ, RS, AE, performed the experiments. GC provided significant technical
365 assistance. *ns957* was isolated by PG and MW in the laboratory of SS. We thank members of the Ghose
366 lab for comments on the manuscript. Some strains were provided by the CGC, which is funded by NIH
367 Office of Research Infrastructure Programs (P40 OD010440).

368

369 **Funding:**

370 PG is a Cancer Prevention Research Institute of Texas (CPRIT) Scholar in Cancer Research (RR100091)
371 and is also funded by a National Institutes of Health-National Institute of General Medical Sciences
372 Maximizing Investigators' Research Award (MIRA) (R35GM142489). NR was supported by NIH SURF
373 Supplemental Award 3R35GM142489-02S2. KJ was funded by NIH Diversity Supplement Program
374 Award 3R35GM142489-02S1, 3R35GM142489-03S1. MW received funding from The Rockefeller
375 University Summer "Gateways to The Laboratory' Program. SS was funded by NIH grants R01HD103610
376 and R35NS105094.

377

378 **Figure Legends:**

379

380 **Figure 1. EOR-1/PLZF promotes CCE cell-autonomously. (A-D)** Stages of CCE**.** IMA, intact mature
381 cell; BD, beading, detached; SDR, soma-distal retracted; SDD, soma, distal degrading. n = 10 biologically

independent animals each with similar results. **(E)** Mutant *ns957* at L1 stage showing persisting TSC soma. n = 10 biologically independent animals each with similar results **(F)** Quantification of *ns957* CCE defects. Data are mean +/_ s.e.m. Statistics: two-tailed unpaired student's t-test, see Supplementary Table 3 for individual P values. **(G-G'')** Enlarged view of *ns957* persisting soma to show DIC view. **(I)** Gene structure of *eor-1*. **(J)** Quantification of *eor-1* fosmid DNA rescue of *ns957*, n=50. (**K)** Quantification CCE defects of other *eor-1* alleles, n=150. **(L, L')** Quantification of CCE defects of additional *eor-1* mutant alleles. **(M)** *eor-1* TSC-specific rescue, n=150. **(N)** *eor-1* expression, *eor-1* promoter-driven mKate2. n = 10 biologically independent animals each with similar results**.** Scale bar, 5 μm. Data are mean +/ s.e.m. Statistics: two-tailed unpaired student's t-test, see Supplementary Table 3 for individual P values.

Figure 2. EOR-1/PLZF functions in CCE with its known partners but likely downstream of CED-3/Caspase. (A) CCE defects across *eor-1* alleles and *eor-2*, *mau-2* and *swsn-1* mutants. Persisting TSC soma phenotypes in **(B, C)** *eor-2(cs42)*, **(D, E)** *mau-2 (qm160)* n = 10 biologically independent animals each with similar results and **(F, G)** *swsn-1 (ku355)* n = 5 biologically independent animals each with similar results. The TSC remains intact at L1 in both *ced-3 (n717)* **(H)** and *ced-4 (n1162); eor-1(cs28)* **(I)** n = 10 biologically independent animals each with similar results**.** Scale bar, 5 μm. n=150 for statistics. Data are mean +/_ s.e.m Statistics: two-tailed unpaired student's t-test, see Supplementary Table 3 for individual P values.

Figure 3. Loss of EOR-1/PLZF causes corpse arrest late in CCE progression. CCE of TSC (membrane marker) in wild-type (**A-F"**) and *eor-1(cs28)* (**I-P''**) mutants showing progression of soma elimination. Left-most panels show whole cell. (**A-B"**) IMA stage in wild-type. n = 10 biologically independent animals each with similar results, (**C-D"**) BA stage in wild-type, n = 8 biologically independent animals each with similar results, (**E-F"**) SDR stage in wild-type, n = 10 biologically independent animals each with similar results, (**G-H"**) SDD stage in wild-type, n = 10 biologically independent animals each with similar results. (**I-J"**) *eor-1 (cs28)* IMA n = 8 biologically independent animals each with similar results, (**K-L"**) *eor-1 (cs28)* BA n = 6 biologically independent animals each with similar results, (M-N") *eor-1 (cs28)* SDR n = 10 biologically independent animals each with similar results, (**O-P"**) *eor-1 (cs28)* SDD n = 10 biologically independent animals each with similar results Scale bar, 5 μm.

Figure 4. The cell corpse of *eor-1* mutants is not internalized by the neighboring phagocyte. Enlarged view of TSC soma at L1 in *ced-3(n717)* (**A-A"**), *ced-12(ky149)* (**B-B"**)**,** *eor-1(ok1127)* (C-C"), *eor-1; ced-12* (**D-D"**), (**E-G**) Test for TSC soma corpse (green) internalization for *eor-1 (cs28)* mutant L1 *larvae* by phagocyte (magenta) at different planes of the phagocyte (upper, middle, lower). n = 10 biologically independent animals each with similar results. Scale bar, 5 μm.

417

418 **Figure 5.EOR-1/PLZF-1 positively regulates *wah-1*/Aif transcription to promote CCE. (A)** *wah-*
419 *1(allele)* CCE defect of TSC at L1 n = 10 biologically independent animals each with similar results. **(B)**
420 Quantification of *wah-1* mutant defect compared to *eor-1* and *wah-1; eor-1* double mutant. **(C)** Graph of
421 TSC-specific rescue of *wah-1* mutant phenotype. Endogenous *wah-1* expression intensity in wild-type
422 **(D)**, *eor-1* **(E)**, *mau-2* **(F)** and *swsn-1* **(G)** mutants. **(H)** Quantification of *wah-1* expression. n = 10
423 biologically independent animals each with similar results. Scale bar, 5 μm. Statistics: two-tailed unpaired
424 student's t-test for scoring and Mann Whittney U test for fluorescence intensity, see Supplementary Table
425 3 for individual P values.

426

427 **Figure 6. The cell corpse of *wah-1* mutants is not internalized and may function at the plasma**
428 **membrane. (A-H")** CCE progression in *wah-1(gk5392).* (**A-B"**) IMA *wah-1 (gk5392)* n = 4 biologically
429 independent animals each with similar results**,** (**C-D"**) BA *wah-1 (gk5392)* n = 5 biologically independent
430 animals each with similar results, (**E-F"**) SDR *wah-1 (gk5392)* n = 4 biologically independent animals
431 each with similar results, (**G-H"**) SDD *wah-1 (gk5392)* n = 3 biologically independent animals each with
432 similar results **(I-K)** TSC and soma-phagocyte dual marker strain in *wah-1* mutant L1 showing failure in
433 TSC corpse internalization. **(L)** L1 *scrm-1* mutant showing persisting TSC soma and exaggerated nuclei.
434 n = 10 biologically independent animals each with similar results. **(M)** Quantification of *scrm-1* mutant
435 defect. Scale bar, 5 μm. Statistics: two-tailed unpaired student's t-test, see Supplementary Table 3 for
436 individual P values.

437

438 **Figure 7. WAH-1 may promote nuclear degradation of the TSC soma corpse at phagolysosomal**
439 **stage. (A)** Quantification of *cps-6(ok1718)* and *nuc-1(e1382)* CCE defect of TSC (soma persistence) at
440 L1. **(B)** Images of these defects. **(D)** Test for soma corpse internalization for *cps-6(ok1718)* across
441 phagocyte planes (upper, middle lower)**.** Localization of phagocyte GFP::RAB-5 **(G-G"),** GFP**::**RAB-7 **(H-**
442 **H")** and LAAT-1:mCherry **(I'-I")** relative to TSC corpse of *cps-6(ok1718)* mutant at L1 stage. n = 10
443 biologically independent animals each with similar results. Scale bar, 5 μm. Statistics: two-tailed unpaired
444 student's t-test, see Supplementary Table 3 for individual P values.

445

446 **Figure 8. WAH-1 exhibits defined spatiotemporal dynamics during CCE progression correlated**
447 **with its function.** TSCp::WAH-1::mCherry and TSCp::mito::GFP localization during CCE IMA **(A**), BA
448 (**B**), SDR (**C**) and SDD (**D**) stages in wild-type embryos. TSCp::mKate2-PH (membrane).
449 TSCp::mito::GFP localization (different animal) during CCE IMA **(E**), BA (**F**), SDR (**G**) and SDD (**H**) stages
450 in wild-type embryos. Relative position of TSC soma versus soma phagocyte (upper, middle and lower

phagocyte planes) at different CCE stages, IMA (**I, J-L**), BD (**M, N-P**), SDR (**Q, R-T**) and SDD (**U, V-X**). n = 10 biologically independent animals each with similar results for A-D. Scale bar, 5 μm.

Figure 9. Model. EOR-1-regulated WAH-1 translocates to different TSC soma sub-compartments to sequentially promote corpse internalization and resolution.

Supplemental Tables:

Supplemental Table 1. Plasmids used in this study.

Supplemental Table 2. Strains and Transgenes used in this study.

Supplemental Table 3. Statistics and P values.

Supplemental Movies:

Supplemental Movie S1. Test for TSC soma internalization of *eor-1 (cs28)* mutants. Green, TSC membrane, Magenta, phagocyte cytosolic marker.

Supplemental Movie S2. Test for TSC soma internalization of *wah-1(gk5392)* mutants. Green, TSC membrane, Magenta, phagocyte cytosolic marker.

Supplemental Movie S3. Test for TSC soma internalization of *cps-6(ok1718)* mutants. Green, TSC membrane, Magenta, phagocyte cytosolic marker.

References

1. Kerr JF, Wyllie AH, Currie AR. Apoptosis: a basic biological phenomenon with wide-ranging implications in tissue kinetics. Br J Cancer. 1972;26(4):239-57.
2. Nonomura K, Yamaguchi Y, Hamachi M, Koike M, Uchiyama Y, Nakazato K, et al. Local apoptosis modulates early mammalian brain development through the elimination of morphogen-producing cells. Dev Cell. 2013;27(6):621-34.
3. Lucantoni F, Salvucci M, Dussmann H, Lindner AU, Lambrechts D, Prehn JHM. BCL(X)L and BCL2 increase the metabolic fitness of breast cancer cells: a single-cell imaging study. Cell Death Differ. 2021;28(5):1512-31.
4. Wang Q, Wang Y, Ding J, Wang C, Zhou X, Gao W, et al. A bioorthogonal system reveals antitumour immune function of pyroptosis. Nature. 2020;579(7799):421-6.
5. Jolly PD, Smith PR, Heath DA, Hudson NL, Lun S, Still LA, et al. Morphological evidence of apoptosis and the prevalence of apoptotic versus mitotic cells in the membrana granulosa of ovarian follicles during spontaneous and induced atresia in ewes. Biol Reprod. 1997;56(4):837-46.

485 6. Saraste A, Pulkki K. Morphologic and biochemical hallmarks of apoptosis. Cardiovasc Res.
486 2000;45(3):528-37.
487 7. Zou H, Henzel WJ, Liu X, Lutschg A, Wang X. Apaf-1, a human protein homologous to C. elegans
488 CED-4, participates in cytochrome c-dependent activation of caspase-3. Cell. 1997;90(3):405-13.
489 8. Vaux DL, Cory S, Adams JM. Bcl-2 gene promotes haemopoietic cell survival and cooperates with
490 c-myc to immortalize pre-B cells. Nature. 1988;335(6189):440-2.
491 9. Ohno H, Takimoto G, McKeithan TW. The candidate proto-oncogene bcl-3 is related to genes
492 implicated in cell lineage determination and cell cycle control. Cell. 1990;60(6):991-7.
493 10. Tait SW, Ichim G, Green DR. Die another way--non-apoptotic mechanisms of cell death. J Cell Sci.
494 2014;127(Pt 10):2135-44.
495 11. Arandjelovic S, Ravichandran KS. Phagocytosis of apoptotic cells in homeostasis. Nat Immunol.
496 2015;16(9):907-17.
497 12. Poon IK, Lucas CD, Rossi AG, Ravichandran KS. Apoptotic cell clearance: basic biology and
498 therapeutic potential. Nat Rev Immunol. 2014;14(3):166-80.
499 13. Savill J, Fadok V, Henson P, Haslett C. Phagocyte recognition of cells undergoing apoptosis.
500 Immunol Today. 1993;14(3):131-6.
501 14. Park SY, Kim IS. Engulfment signals and the phagocytic machinery for apoptotic cell clearance.
502 Exp Mol Med. 2017;49(5):e331.
503 15. Lu N, Zhou Z. Membrane trafficking and phagosome maturation during the clearance of
504 apoptotic cells. Int Rev Cell Mol Biol. 2012;293:269-309.
505 16. Kinchen JM, Ravichandran KS. Phagosome maturation: going through the acid test. Nat Rev Mol
506 Cell Biol. 2008;9(10):781-95.
507 17. Fairn GD, Grinstein S. How nascent phagosomes mature to become phagolysosomes. Trends
508 Immunol. 2012;33(8):397-405.
509 18. Pauwels AM, Trost M, Beyaert R, Hoffmann E. Patterns, Receptors, and Signals: Regulation of
510 Phagosome Maturation. Trends Immunol. 2017;38(6):407-22.
511 19. Ellis HM, Horvitz HR. Genetic control of programmed cell death in the nematode C. elegans.
512 Cell. 1986;44(6):817-29.
513 20. Abraham MC, Lu Y, Shaham S. A morphologically conserved nonapoptotic program promotes
514 linker cell death in Caenorhabditis elegans. Dev Cell. 2007;12(1):73-86.
515 21. Ellis RE, Jacobson DM, Horvitz HR. Genes required for the engulfment of cell corpses during
516 programmed cell death in Caenorhabditis elegans. Genetics. 1991;129(1):79-94.
517 22. Guo P, Hu T, Zhang J, Jiang S, Wang X. Sequential action of Caenorhabditis elegans Rab GTPases
518 regulates phagolysosome formation during apoptotic cell degradation. Proc Natl Acad Sci U S A.
519 2010;107(42):18016-21.
520 23. Raiders S, Black EC, Bae A, MacFarlane S, Klein M, Shaham S, et al. Glia actively sculpt sensory
521 neurons by controlled phagocytosis to tune animal behavior. Elife. 2021;10.
522 24. Fazeli G, Stetter M, Lisack JN, Wehman AM. C. elegans Blastomeres Clear the Corpse of the
523 Second Polar Body by LC3-Associated Phagocytosis. Cell Rep. 2018;23(7):2070-82.
524 25. Haley R, Wang Y, Zhou Z. The small GTPase RAB-35 defines a third pathway that is required for
525 the recognition and degradation of apoptotic cells. PLoS Genet. 2018;14(8):e1007558.
526 26. Kutscher LM, Keil W, Shaham S. RAB-35 and ARF-6 GTPases Mediate Engulfment and Clearance
527 Following Linker Cell-Type Death. Dev Cell. 2018;47(2):222-38 e6.

27. Ghose P, Rashid A, Insley P, Trivedi M, Shah P, Singhal A, et al. EFF-1 fusogen promotes phagosome sealing during cell process clearance in Caenorhabditis elegans. Nat Cell Biol. 2018;20(4):393-9.
28. Chiorazzi M, Rui L, Yang Y, Ceribelli M, Tishbi N, Maurer CW, et al. Related F-box proteins control cell death in Caenorhabditis elegans and human lymphoma. Proc Natl Acad Sci U S A. 2013;110(10):3943-8.
29. Jiang HS, Ghose P, Han HF, Wu YZ, Tsai YY, Lin HC, et al. BLMP-1 promotes developmental cell death in C. elegans by timely repression of ced-9 transcription. Development. 2021;148(20).
30. Maurer CW, Chiorazzi M, Shaham S. Timing of the onset of a developmental cell death is controlled by transcriptional induction of the C. elegans ced-3 caspase-encoding gene. Development. 2007;134(7):1357-68.
31. Conradt B, Wu YC, Xue D. Programmed Cell Death During Caenorhabditis elegans Development. Genetics. 2016;203(4):1533-62.
32. Sulston JE, Schierenberg E, White JG, Thomson JN. The embryonic cell lineage of the nematode Caenorhabditis elegans. Dev Biol. 1983;100(1):64-119.
33. Ziegler U, Groscurth P. Morphological features of cell death. News Physiol Sci. 2004;19:124-8.
34. Hoeppner DJ, Spector MS, Ratliff TM, Kinchen JM, Granat S, Lin SC, et al. eor-1 and eor-2 are required for cell-specific apoptotic death in C. elegans. Dev Biol. 2004;274(1):125-38.
35. Shinkai Y, Kuramochi M, Doi M. Regulation of chromatin states and gene expression during HSN neuronal maturation is mediated by EOR-1/PLZF, MAU-2/cohesin loader, and SWI/SNF complex. Sci Rep. 2018;8(1):7942.
36. Malin JA, Kinet MJ, Abraham MC, Blum ES, Shaham S. Transcriptional control of non-apoptotic developmental cell death in C. elegans. Cell Death Differ. 2016;23(12):1985-94.
37. Howell K, Arur S, Schedl T, Sundaram MV. EOR-2 is an obligate binding partner of the BTB-zinc finger protein EOR-1 in Caenorhabditis elegans. Genetics. 2010;184(4):899-913.
38. Niu W, Lu ZJ, Zhong M, Sarov M, Murray JI, Brdlik CM, et al. Diverse transcription factor binding features revealed by genome-wide ChIP-seq in C. elegans. Genome Res. 2011;21(2):245-54.
39. Troulinaki K, Buttner S, Marsal Cots A, Maida S, Meyer K, Bertan F, et al. WAH-1/AIF regulates mitochondrial oxidative phosphorylation in the nematode Caenorhabditis elegans. Cell Death Discov. 2018;4:2.
40. Wang X, Wang J, Gengyo-Ando K, Gu L, Sun CL, Yang C, et al. C. elegans mitochondrial factor WAH-1 promotes phosphatidylserine externalization in apoptotic cells through phospholipid scramblase SCRM-1. Nat Cell Biol. 2007;9(5):541-9.
41. Wang X, Yang C, Chai J, Shi Y, Xue D. Mechanisms of AIF-mediated apoptotic DNA degradation in Caenorhabditis elegans. Science. 2002;298(5598):1587-92.
42. Gerstein MB, Lu ZJ, Van Nostrand EL, Cheng C, Arshinoff BI, Liu T, et al. Integrative analysis of the Caenorhabditis elegans genome by the modENCODE project. Science. 2010;330(6012):1775-87.
43. Parrish J, Li L, Klotz K, Ledwich D, Wang X, Xue D. Mitochondrial endonuclease G is important for apoptosis in C. elegans. Nature. 2001;412(6842):90-4.
44. Ma A, Feng Q, Li P, Yuan L, Xiao H. SCAV-3 affects apoptotic cell degradation in Caenorhabditis elegans. FEBS Open Bio. 2023;13(5):867-80.
45. Wu YC, Stanfield GM, Horvitz HR. NUC-1, a caenorhabditis elegans DNase II homolog, functions in an intermediate step of DNA degradation during apoptosis. Genes Dev. 2000;14(5):536-48.

Time

Rather et. al, FIGURE 1

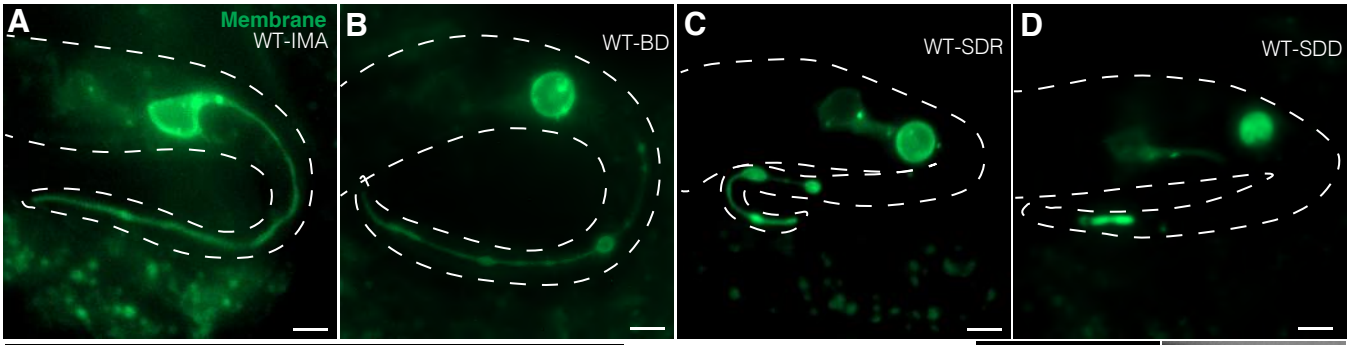

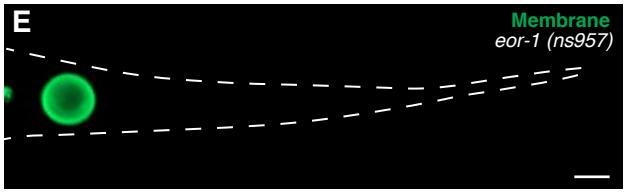

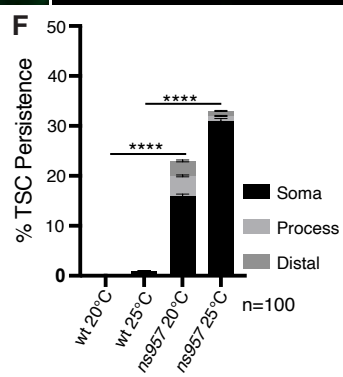

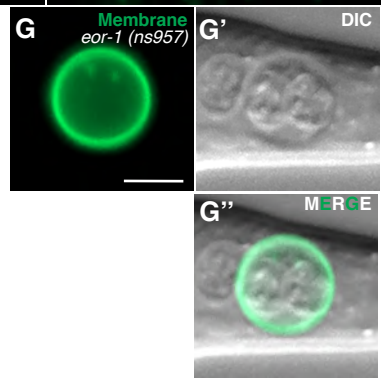

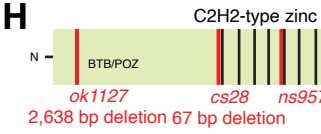

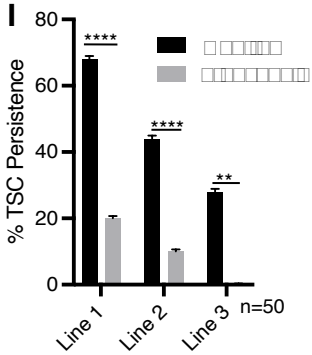

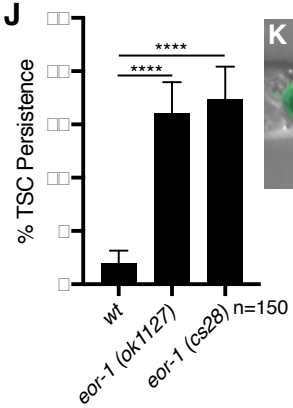

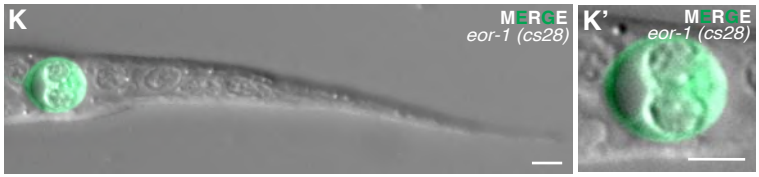

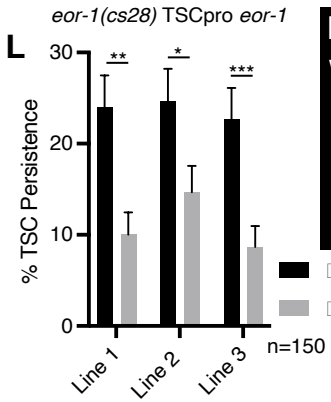

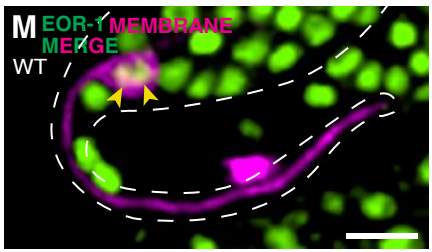

Rather et. al, FIGURE 2

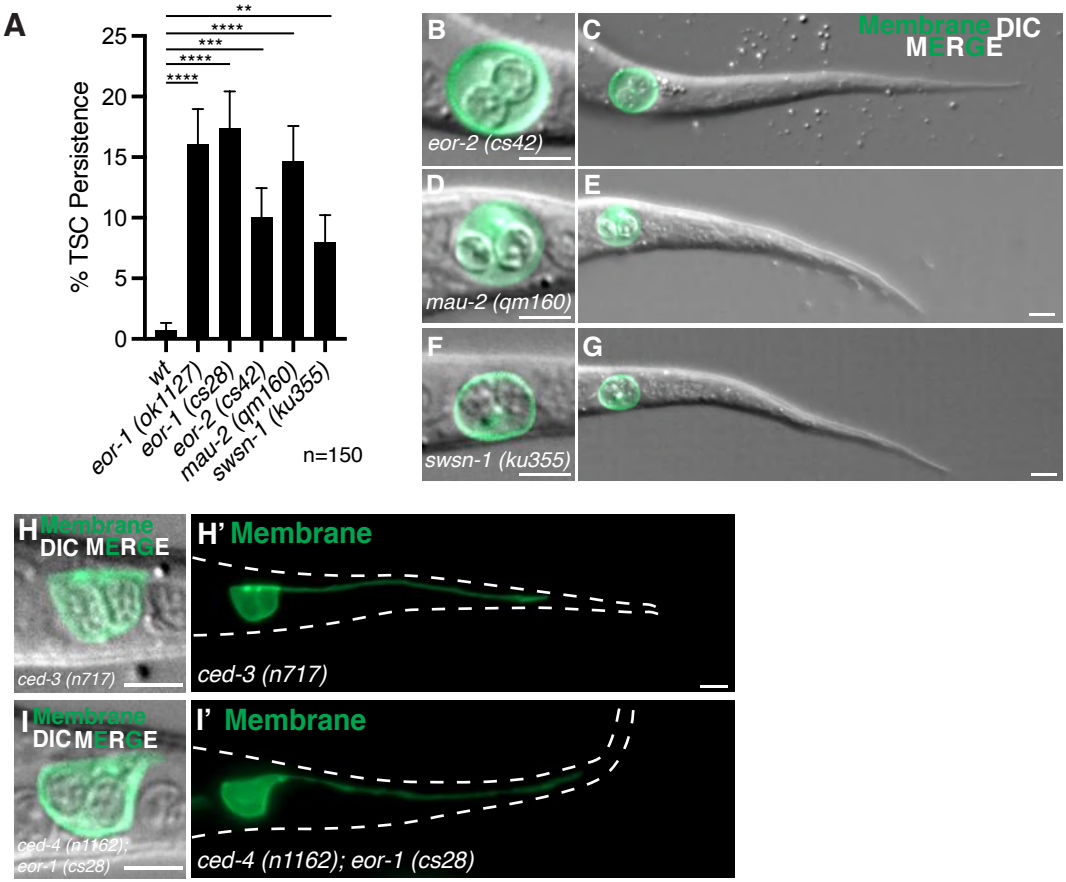

Rather et. al, FIGURE 3

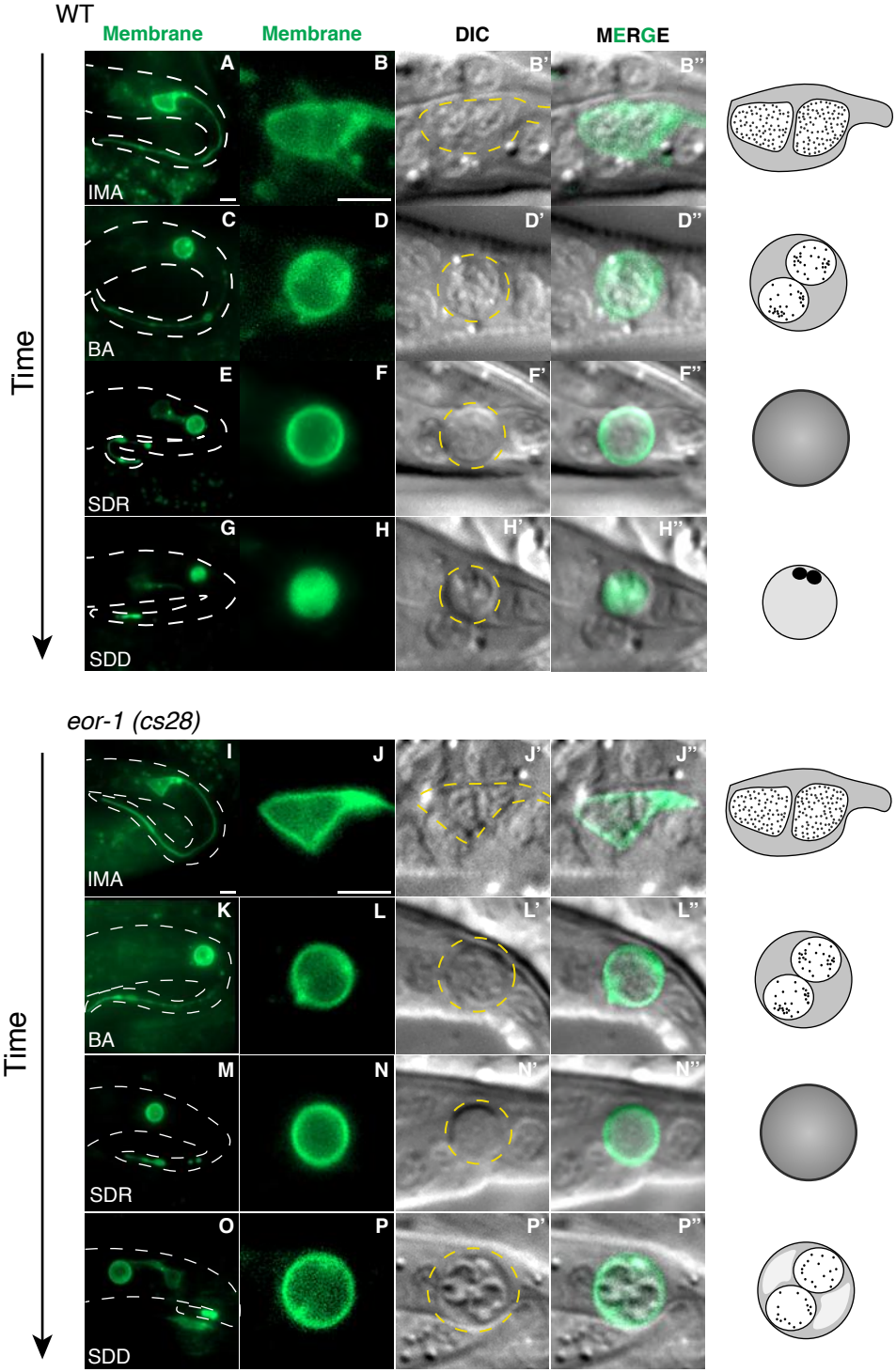

Rather et. al, FIGURE 4

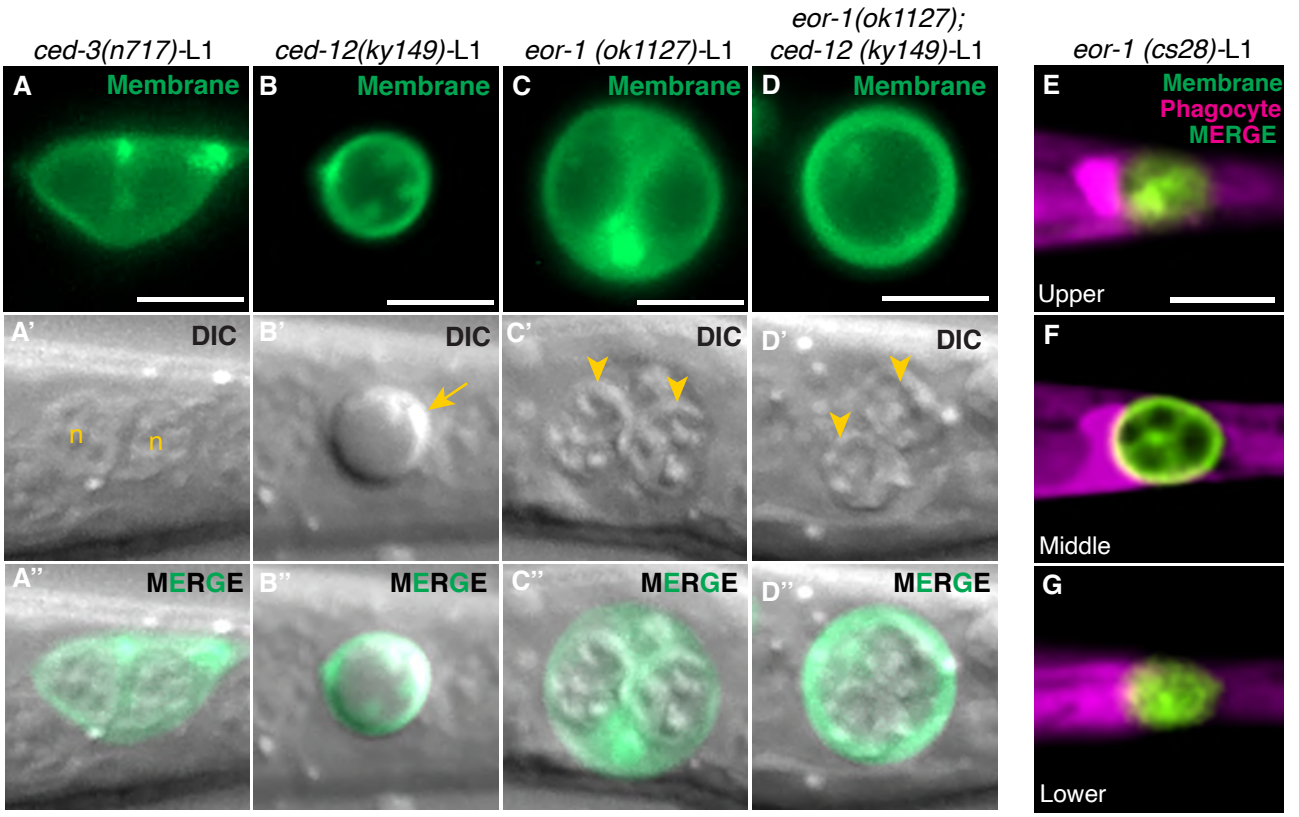

Rather et. al, FIGURE 5

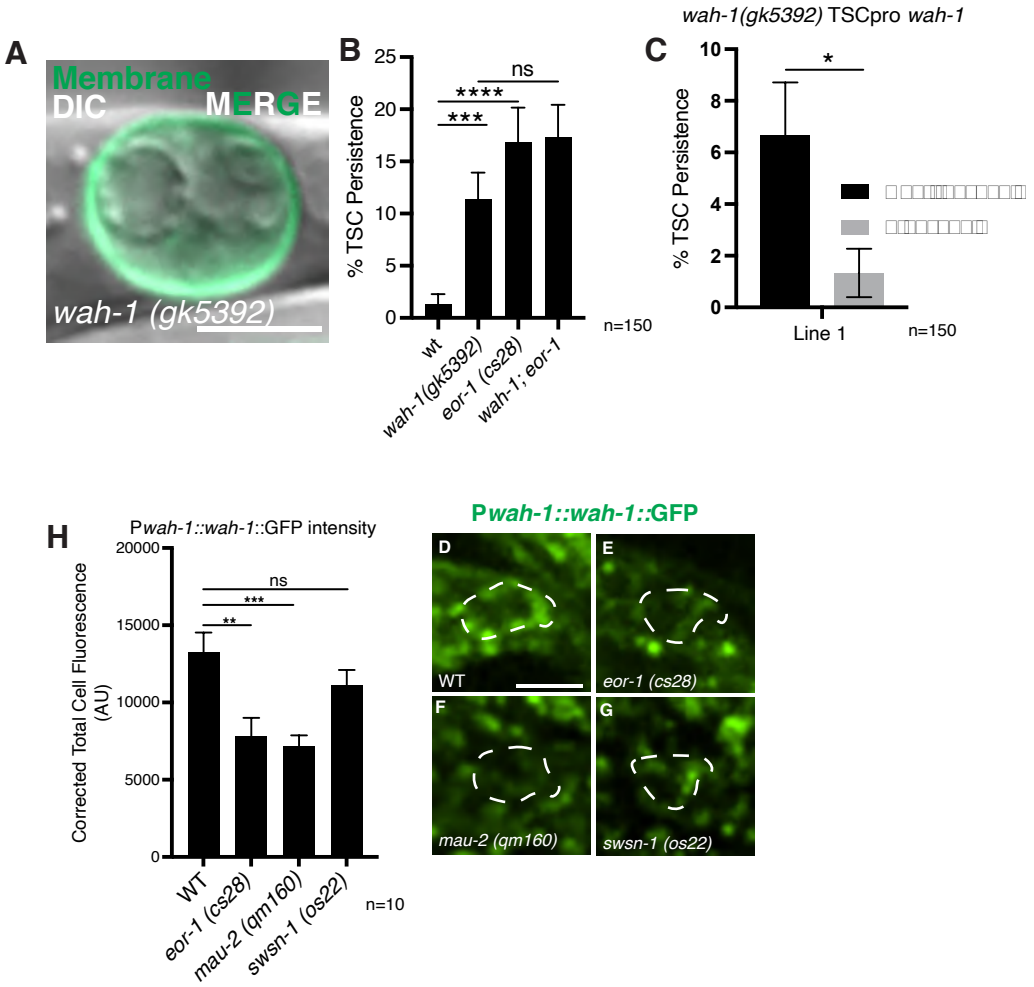

Rather et. al, FIGURE 6

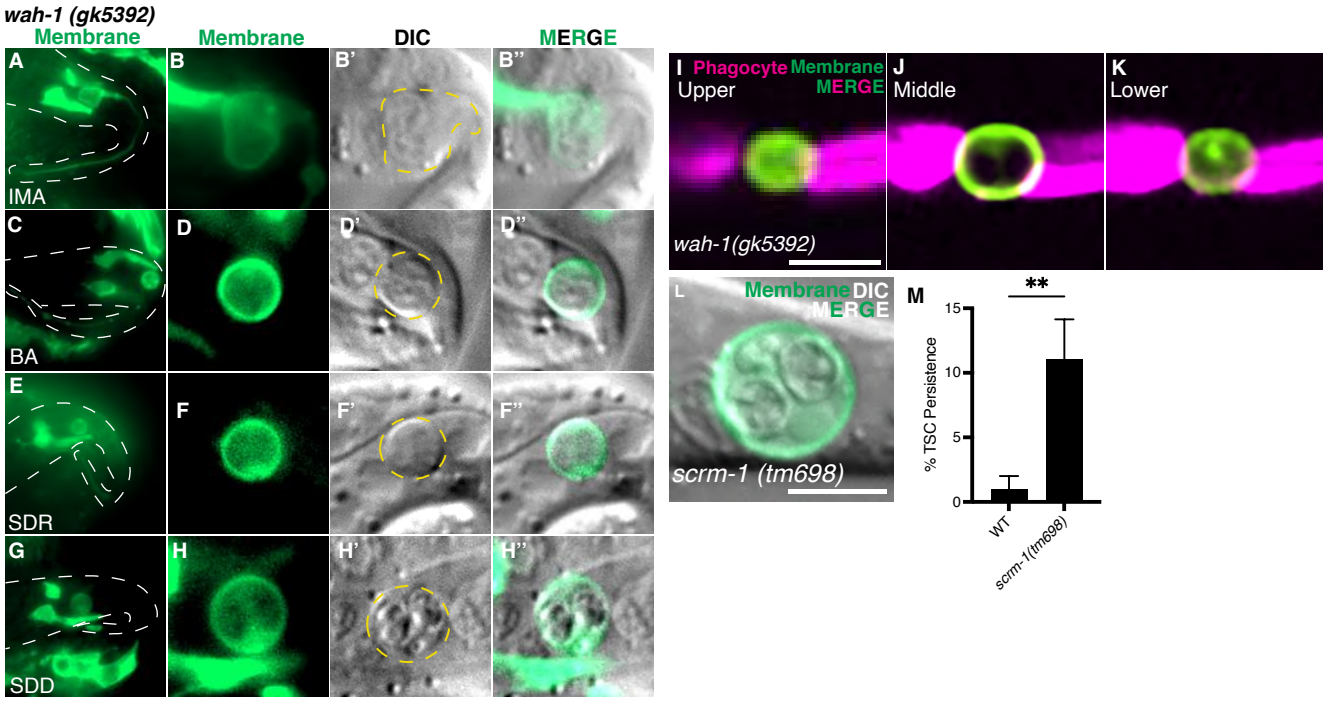

Rather et. al, FIGURE 7

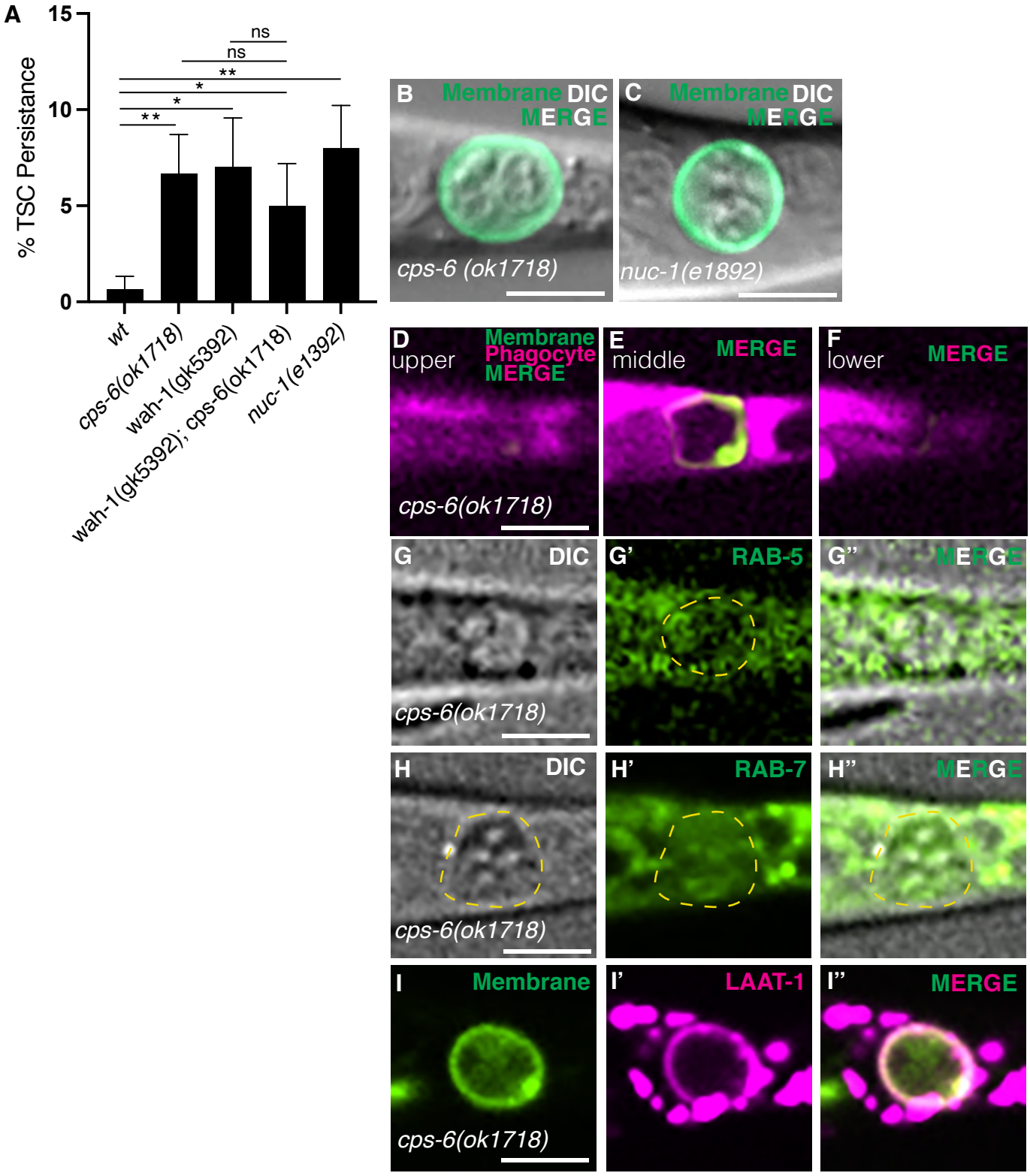

Rather et. al, FIGURE 8

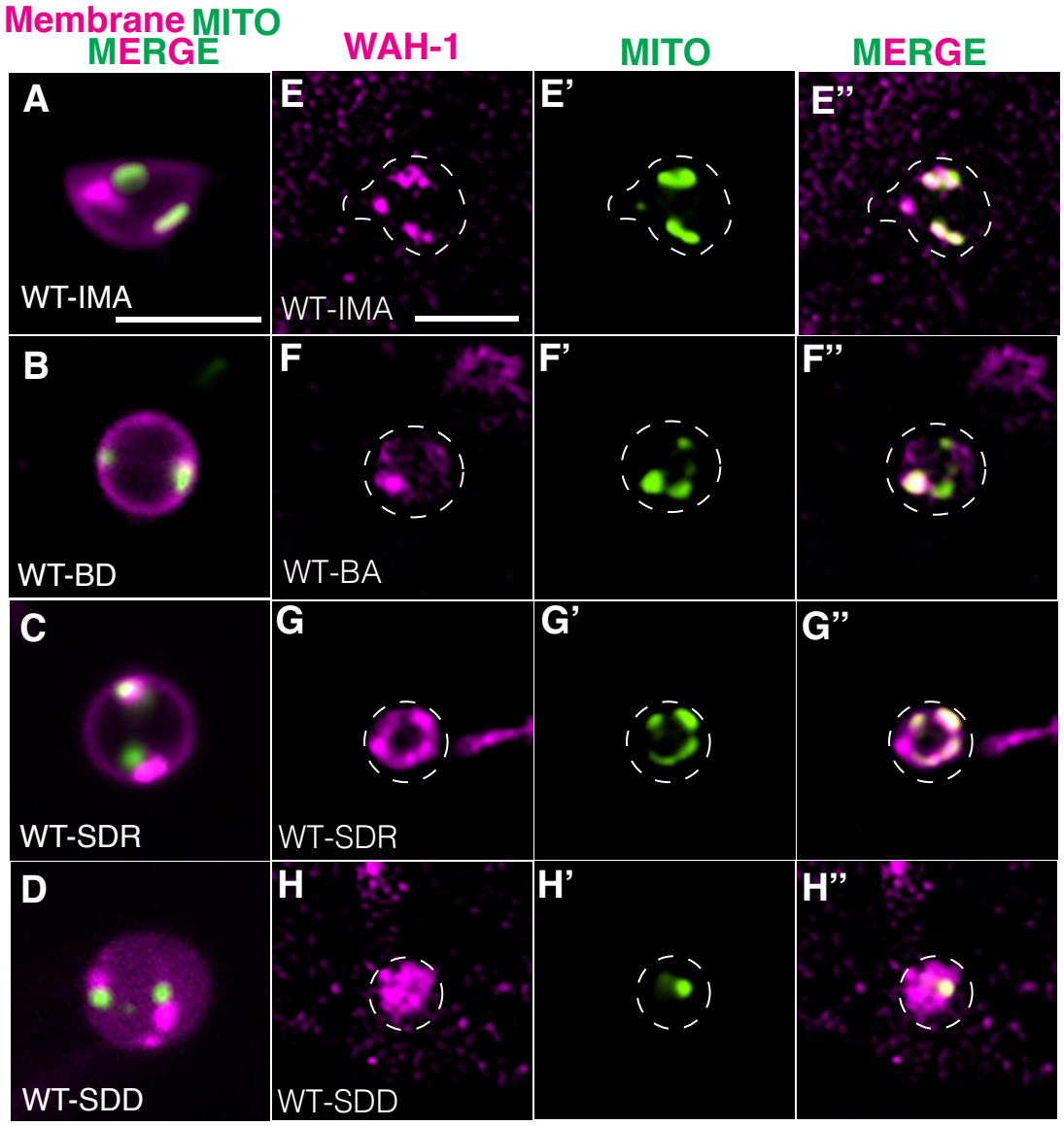

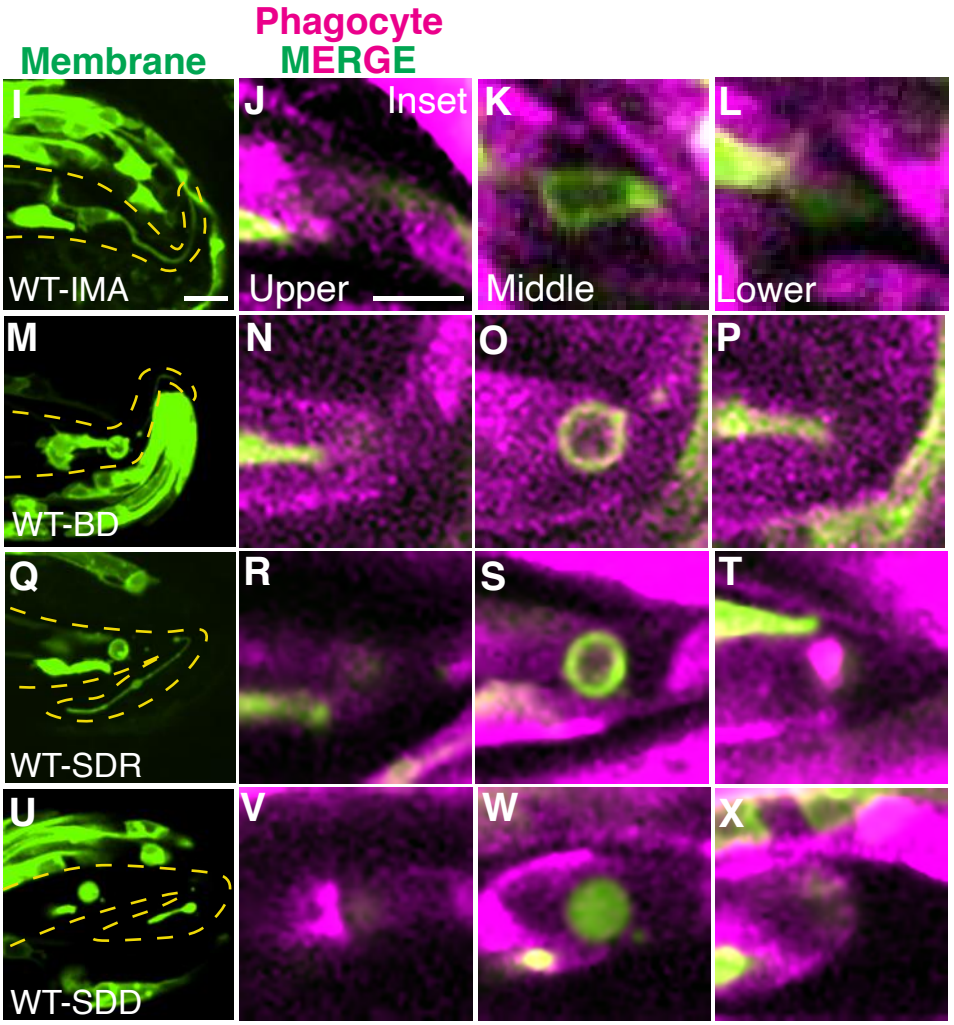
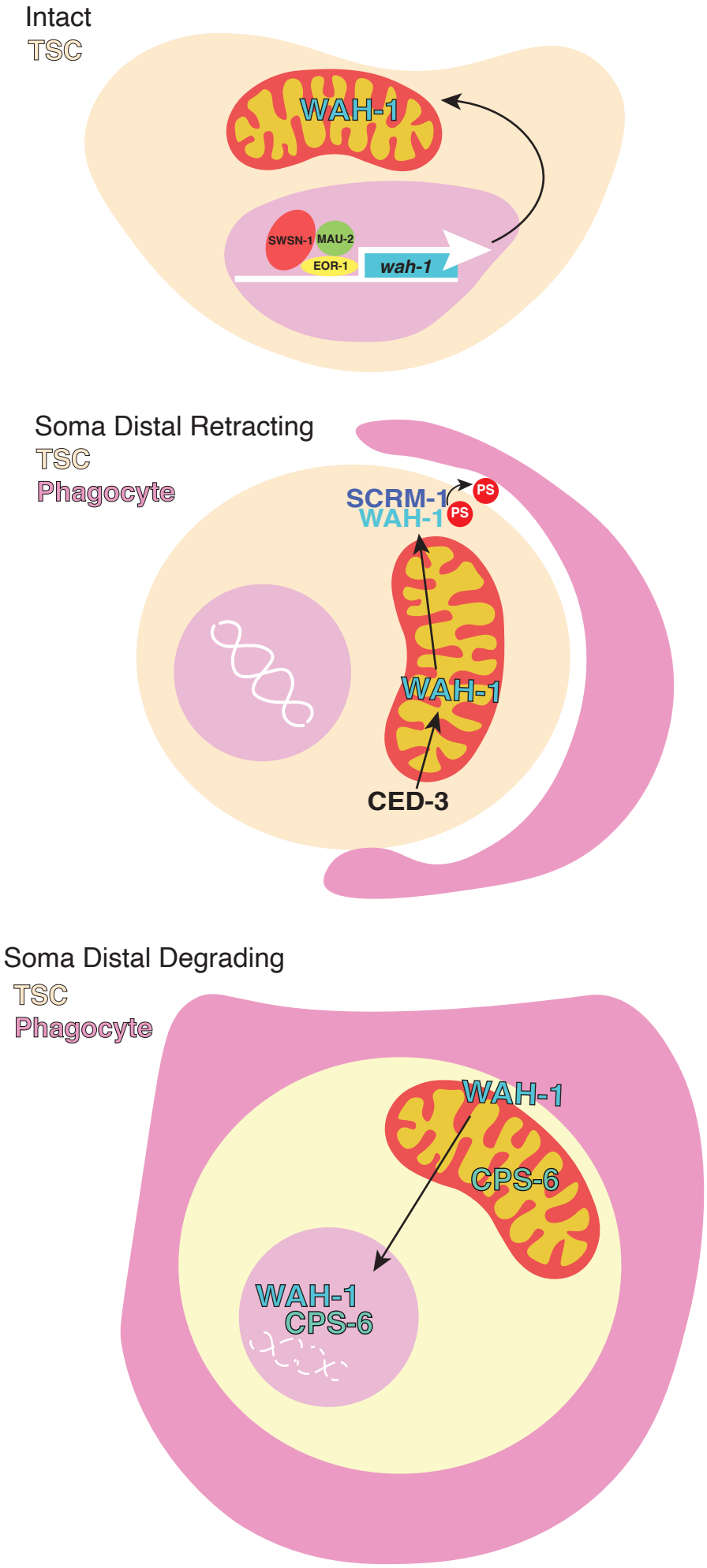
Rather et al Figure 9